Case Studies in Thermal Engineering 35 (2022) 102046

Contents lists available at ScienceDirect

Case Studies in Thermal Engineering

journal homepage: www.elsevier.com/locate/csite

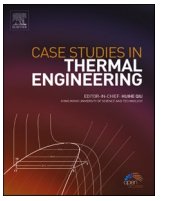

Numerical simulation of a thermally enhanced EMHD flow of a heterogeneous micropolar mixture comprising (60%)-ethylene glycol (EG), (40%)-water (W), and copper oxide nanomaterials (CuO)

Nehad Ali Shah [a], Abderrahim Wakif [b], Essam R. El-Zahar [c,d], Sohail Ahmad [e], Se-Jin Yook [f,*]

[a] Department of Mechanical Engineering, Sejong University, Seoul, 05006, South Korea
[b] Laboratory of Mechanics, Faculty of Sciences Aïn Chock, Hassan II University of Casablanca, Casablanca, 20000, Morocco
[c] Department of Mathematics, College of Science and Humanities in Al-Kharj, Prince Sattam bin Abdulaziz University, P.O. Box 83, Al-Kharj, 11942, Saudi Arabia
[d] Department of Basic Engineering Science, Faculty of Engineering, Menoufia University, Shebin El-Kom, 32511, Egypt
[e] Department of Mathematics, COMSATS University Islamabad, Attock Campus, Pakistan
[f] School of Mechanical Engineering, Hanyang University, 222 Wangsimni-ro, Seongdong-gu, Seoul, 04763, South Korea

ARTICLE INFO

Keywords:
EMHD micropolar Nanofluid flow
Buongiorno's model
Riga plate
Convective heating
Adjustable heat source

ABSTRACT

In the past decades, the thermal and rheological properties of nanofluids have attracted much attention from many investigators due to their numerous applications as promising enhanced working fluids. The present numerical analysis intended to evidence the main hydro-thermal and mass transport appearances featuring the convective flows of an exceptional non-homogeneous micropolar mixture (i.e., 60% of ethylene glycol, 40% of pure water, and copper oxide nanomaterials) over an impermeable horizontal electromagnetic surface (i.e., Riga plate), which is heated convectively in the presence of a particular variable heat source. For this purpose, several admissible physical theories and hypotheses are adopted herein to derive the foremost conservation equations based on the renovated Buongiorno's formulation and some more realistic boundary conditions. Further, the leading partial differential equations (PDEs) are transformed into a system of ordinary differential equations (ODEs), which are tacked thereafter numerically using an efficient GDQNRM procedure. After performing multiple validations with the recent literature results, the aspects of the studied EMHD convective micropolar nanofluid flow are spotted accordingly and then discussed comprehensively via multiple figures and tables. As prominent results, it is found that the micropolarity and electrically conducting trends of the nanofluidic medium play an important role in the hastening of the nanofluid motion. Also, it is explored that the thermally enhancing influence of the thermophoresis diffusive mechanism can be reinforced more by the existence of an internal heat source along with an appropriate convective heating process.

* Corresponding author.
E-mail addresses: nehadali199@sejong.ac.kr (N.A. Shah), wakif.abderrahim@gmail.com (A. Wakif), er.elzahar@psau.edu.sa (E.R. El-Zahar), drsohailahmad@ciit-attock.edu.pk (S. Ahmad), ysjnuri@hanyang.ac.kr (S.-J. Yook).

https://doi.org/10.1016/j.csite.2022.102046
Received 18 September 2021; Received in revised form 31 March 2022; Accepted 15 April 2022
Available online 21 April 2022

Nomenclature

General Symbols and Abbreviations

a_0	Size of electrodes and magnets, m
BCs	Dimensional/Unitless boundary conditions
$[BCs_{\widehat{(u,v)}}, BCs_f]$	Dimensional/Unitless boundary conditions for the velocity components
$[BCs_{\widehat{N}}, BCs_g]$	Dimensional/Unitless boundary conditions for the micro-rotation velocity
$[BCs_{\widehat{T}}, BCs_\theta]$	Dimensional/Unitless boundary conditions for the temperature
$[BCs_{\widehat{C}}, BCs_\chi]$	Dimensional/Unitless for the nanoparticles' molar concentration
$\widehat{C}(\widehat{x},\widehat{y})$	Dimensional distribution of the nanoparticles' molar concentration, $mol\,m^{-3}$
C_∞	Free-stream nanoparticles' molar concentration, $mol\,m^{-3}$
$[D_B, D_T]$	Mass diffusive coefficients, $m^2 s^{-1}$
Eqs	Dimensional/Unitless leading equations
$[Eqs_{\widehat{(u,v)}}, Eqs_f]$	Dimensional/Unitless equations for the velocity components
$[Eqs_{\widehat{N}}, Eqs_g]$	Dimensional/Unitless equations for the micro-rotation velocity
$[Eqs_{\widehat{T}}, Eqs_\theta]$	Dimensional/Unitless equations for the temperature
$[Eqs_{\widehat{C}}, Eqs_\chi]$	Dimensional/Unitless equations for the nanoparticles' molar concentration
$[f(\eta), f'(\eta)]$	Velocity functions in dimensionless forms
$g(\eta)$	Micro-rotation velocity function in a dimensionless form
h_f	Convective heat transfer coefficient, $W\,m^{-2}K^{-1}$
j_0	Electrical current density Am^{-2}
j	Micro-inertial factor, m^2
k_B	Boltzmann constant ($k_B = 1.38066 \times 10^{-23} j\,K^{-1}$)
$M(\widehat{x})$	Adjustable magnetization strength, $kg\,s^{-2}A^{-1}$
M_{CuO}	Molar mass of copper oxide nanomaterials, $kg\,mol^{-1}$
$\widehat{N}(\widehat{x},\widehat{y})$	Dimensional field of the micro-rotation velocity, $rad\,s^{-1}$
Q_E	Heat source potency, $W\,m^{-3}K^{-1}$
s	Stretching velocity rate, s^{-1}
$\widehat{T}(\widehat{x},\widehat{y})$	Dimensional distribution of the temperature, K
T_f	Temperature of the heated working fluid, K
T_{ref}	Reference temperature ($T_{ref} = 273K$)
T_∞	Free-stream temperature, K
$[\widehat{u}(\widehat{x},\widehat{y}), \widehat{v}(\widehat{x},\widehat{y})]$	Velocity field, $m\,s^{-1}$
$[\widehat{x},\widehat{y}]$	Cartesian coordinate system, m

Greek Symbols

$\chi(\eta)$	Nanoparticles' molar concentration in a dimensionless form
φ	Nanoparticles' volume fraction
$[\xi,\eta]$	Dimensionless coordinate system
υ	Kinematic viscosity, $m^2 s^{-1}$
$\theta(\eta)$	Temperature function in a dimensionless form
κ	Vortex viscosity, $Pa\,s$

Subscripts

f	Working fluid
hbf	Hybrid base fluid
nf	Nanofluid
CuO	Copper oxide nanoparticles
∞	Free-stream condition
w	Wall characteristic

Superscripts

,	First-order derivative w.r.t. η
, ,	Second-order derivative w.r.t. η
, , ,	Third-order derivative w.r.t. η

1. Introduction

Nowadays, the topic of nanofluid flows has gained remarkable courtesy from pioneering researchers [1–7] owing to the astounding thermal performance of the nanofluidic mixtures and their significant capabilities of changing the happening transport phenomena as well as their evolutionary dynamics. Naturally, many customary liquids possess a feeble thermal conductivity. Hence, it is useless from a practical point of view to choose them as heat transfer fluids in the engineering processes. For this purpose, it is more recommended to insert solid nanoparticles having higher thermal features into a specified base fluid to prepare an efficient biphasic mixture even with the addition of a small volume fraction of solid nanomaterials. Scientifically, the nanofluid terminology was utilized first by Choi [8] in 1995. After that, numerous experimental and theoretical attempts were undertaken in this context to show the importance of employing nanofluids instead of some traditional working liquids as reported by Angayarkanni and Philip [3]. Keeping in mind the practical uses of nanofluids in various technological and industrial sectors [9–13] (e.g., drug delivery, renewable energies, solar energy systems, oil recovery, and cooling of nuclear systems), interesting outcomes have been drawn by eminent researchers [14–22] concerning the prominent thermal performances of nanofluids. Motivated by the applicability and the importance of nanofluids, Acharya et al. [23–26] carried out extensive finite element simulations to deliberate comprehensively the hydro-thermal features of convective flows inside a square/triangular/hexagonal cavity filled by homogeneous water-based nanofluids encompassing alumina or magnetic iron oxide spherical-shaped nanomaterials. Several interesting findings were derived from these numerical examinations regarding the dynamics of nanofluids and their behaviors in different situations. An advanced non-homogeneous nanofluid flow model was formulated by Rasool et al. [27] based on Buongiorno's physical standpoints [28] to inspect the two-dimensional radiative motion of a Maxwell nanofluid over an isothermal stretching sheet in the presence of Lorentz and Darcy-Forchheimer forces. Likewise, Dawar et al. [29] assumed the renovated two-phase nanofluid model to expose the general appearances of tri-dimensional Jeffrey nanofluid flows over a convectively heated bi-stretching surface exhibiting many velocity slip trends. By invoking the Atangana-Baleanu fractional approach, Shah et al. [30] exploited the single-phase nanofluid flow model [31] to examine an unsteady mixed convective flow developed over an isothermally moving vertical plate for a ternary nanofluid incorporating a second-grade fluid along with the silver, copper, and alumina nanoparticles.

Conventionally, the existence of an external magnetic source may affect significantly the dynamics of electrically conducting fluids flowing effectively in its spawned field. However, this magnetic capability of flow control disappears practically in fluids having a low electrical conductance feature due to the feeble strength of the induced current density. Accordingly, when the induced electrical current is of insufficient intensity, an electric field should be applied also to the fluidic medium in this case to ensure a noticeable dynamical impact. Because of this, Gailitis [32] suggested the use of the Riga plate as an electromagnetic actuator to generate Lorentz forces in the stream-wise mode for controlling the motion of weakly conducting fluids. This sophisticated surface is an electromagnetically aligned actuator that involves an array of electrodes and permanent magnets. Among, the main applications of this smart plate include the minimization of wall drag forces as well as the prevention of boundary layer separation and the reduction of mechanical energy. In this context, Wakif et al. [33] demonstrated the possibility of getting a higher thermodynamical entropy generation within a dissipative fluidic medium by strengthening the generated electromagnetic forces during its EMHD (i.e., electro-magneto-hydrodynamic) motion near an isothermally heated Riga plate constrained hydrodynamically by a uniform suction process and energetically by the Joule heating mechanism. In the case of a nanofluid flow geometry, Kumar et al. [34] practiced an efficient implicit Keller box procedure to disclose the significance of a first-order chemical reactive process and thermal radiation on EMHD convective flows of Williamson nanofluids over an irregular Riga plate in the case of zero mass flux and convective heating conditions. Otherwise, Awati et al. [35] proposed a Haar wavelet algorithm to check the results reported previously by Rana and Bhargava [36] for the convective nanofluid flows over a power-law stretching surface. A comprehensive meta-analyses were carried out statistically by Wakif et el. [37] to explore the diverse aspects of nanoparticles in the heat and mass transport phenomena within a nanofluidic medium. To reflect rheologically the micropolarity trend of kerosene and water, Zaib et al. [38] applied the single-phase nanofluid model to evaluate their mixed convective motions towards a Riga plate when these base fluids are saturated by titanium dioxide nanomaterials. By combining the generalized thermal and mass transport laws with the revised version of the two-phase nanofluid approach, Naseem et al. [39] proposed a theoretical model for studying third-grade nanofluid flows over a Riga plate. A spectral quasi-linearization analysis was conducted by Akolade and Tijani [40] to realize a quantitative comparison between the Casson and Williamson rheological models through the three-dimensional flows of their corresponding nanofluids over a Riga plate. Dissimilarly, Rasool and Wakif [41] applied the spectral local linearization method to scrutinize the EMHD mixed convective nanofluid motion near a vertical Riga plate by adopting the second-grade rheological model along with the generalized forms of Fourier's and Fick's laws and the revised two-phase nanofluid formulation. Particularly, Gangadhar et al. [42] pursued the same rheological strategy to examine the bi-phasic dynamics of radiative non-Newtonian nanofluids over a convectively heated Riga plate. Based on a strong theoretical background, Vaidya et al. [43] suggested an advanced dissipative nanofluid flow model with a first-order chemical reaction process to divulge the characteristics of mixed convective nanofluid flows near a vertical Riga plate of variable thickness in the presence of a temperature-dependent heat source.

In fact, despite the great effort expended in the two last decades by the researchers in nanofluid subjects, many achievements remain questionable from the reliability and validity points of view concerning the proposed flow models and the presented findings, in which some happening physical phenomena are still unclear that might be explained consistently based on a rigorous theoretical basis and appropriate nanofluid models. Enlightening by the afore deliberated literature survey, the present numerical examination deals with the proper application of the renovated Buongiorno's approach that has been proposed recently by Wakif et al. [44] to

provide new physical insights on the dynamics of a non-homogeneous micropolar mixture constituted by 60% of ethylene glycol ($C_2H_6O_2$), 40% of water (H_2O), and a certain volume fraction of copper oxide nanoparticles (CuO).

Exclusively, the nanofluid flow problem under consideration is formulated successfully in such a way that the following novelties are integrated into the monitored equations:

1 A novel micropolar non-homogeneous nanofluid model is developed properly.
2 The mathematical description of the nanofluid flow problem is formulated accordingly via the nanoparticles' molar concentration instead of nanoparticles' volume fraction.
3 A significant driven EMHD trend is assured dynamically over a stretching Riga plate.
4 Nield's boundary conditions [45,46] are applied at the Riga plate for the nanoparticles' flux.
5 The micropolar nanofluidic medium is enhanced thermally by a convective heating mechanism.
6 The temperature distribution is adjusted internally through an exponential space- and temperature-dependent heat source.
7 A set of experimental correlations and phenomenological laws are employed as thermophysical expressions for the present micropolar nanofluid.

2. Mathematical and physical backgrounds

The geometry of the proposed two-dimensional EMHD micropolar nanofluid flow model is sketched in a Cartesian system $(\hat{x},\hat{y})$ for the biphasic mixture $CuO-[(60\%)-C_2H_6O_2+(40\%)-H_2O]$ as outlined in Fig. 1. In this scrutinization, the nanofluid flow is established over a horizontal Riga device. Initially, the hybrid base fluid $[(60\%)-C_2H_6O_2+(40\%)-H_2O]$ comprehends a uniform distribution of copper oxide nanomaterials having a spherical-shaped geometry of diameter $d_{CuO}=29nm$, whose volume fraction φ_0 should be ranged mandatory from 0.01 to 0.06. In addition, the following assumptions are considered during this analysis:

– The nanofluidic mixture $CuO-[(60\%)-C_2H_6O_2+(40\%)-H_2O]$ has micropolar and electrical behaviors.
– The proper relationship linking the volume fraction φ of copper oxide nanoparticles and their molar concentration C is given by $\varphi=\frac{M_{CuO}\,C}{\rho_{CuO}}$ [44,47].
– The formulation of the present nanofluid flow problem is expressed in the laminar steady-state based on the two-phase nanofluid approach, the micropolar theory [48], and the boundary layer approximations [49].
– A specific variable heat source is located internally in the nanofluidic medium to provide an additional amount of thermal energy, whose puissance depends on the temperature filed $\widehat{T}(\hat{x},\hat{y})$ and decays exponentially with the variable space $\hat{y}$.
– The effective contribution of Brownian and thermophoretic diffusive phenomena is reflected in the present non-homogeneous flow model.

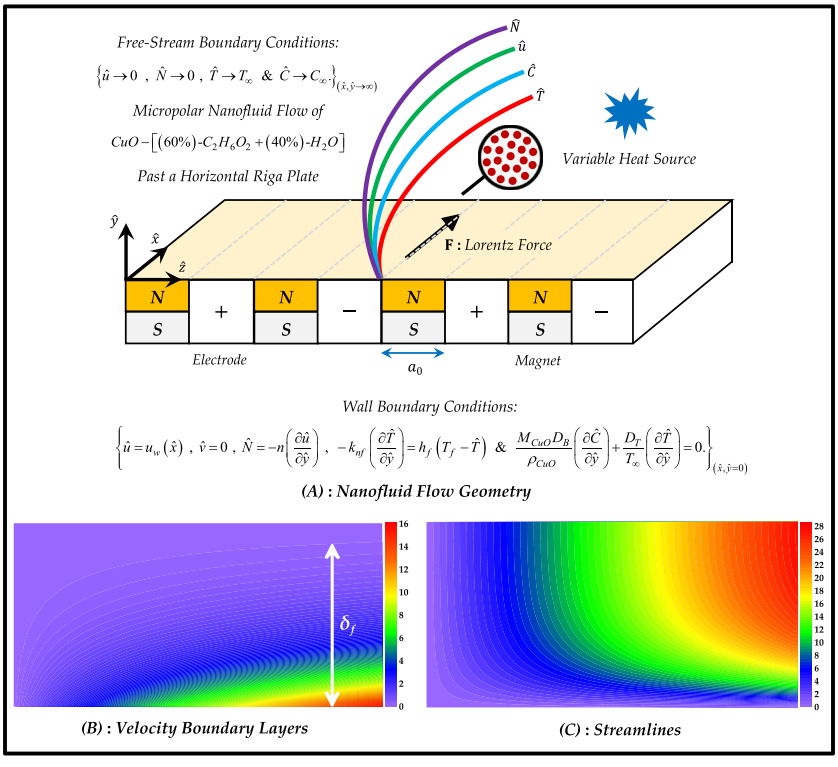

Fig. 1. EMHD micropolar nanofluid flow model.

- The flat planar geometry is stretched horizontally along the $\widehat{x}-$ direction with a variable velocity $u_w(\widehat{x})$, whose expression is given by $u_w(\widehat{x}) = s\widehat{x}$.
- The Riga plate is heated convectively through the temperature T_f of a working fluid, whose characteristic thermal convective coefficient is indicated by h_f.
- The wall molar concentration of nanoparticles $\widehat{C}(\widehat{x}, \widehat{y}=0)$ is determined passively via the vanishing mass flux condition $\left(\frac{\partial \widehat{C}}{\partial \widehat{y}}\right)_{(\widehat{x},\widehat{y}=0)} = -\frac{\rho_{CuO}\, D_T}{M_{CuO}\, D_B T_\infty}\left(\frac{\partial \widehat{T}}{\partial \widehat{y}}\right)_{(\widehat{x},\widehat{y}=0)}$.
- The values of free-stream temperature T_∞ and its corresponding molar concentration C_∞ are preserved constant, whereas the micropolar nanofluid and its micro-elements are kept in a motionless state.

Based on the above considerations and the recent adjustments proposed by Wakif et al. [44] on Buongiorno's formulation [28], the leading PDEs and BCs are listed below as:

$$\left\{ \begin{array}{l} Eq_{\widehat{(u,v)}} : \left\{ \dfrac{\partial \widehat{u}}{\partial \widehat{x}} = -\dfrac{\partial \widehat{v}}{\partial \widehat{y}}\ ,\ \widehat{u}\left(\dfrac{\partial \widehat{u}}{\partial \widehat{x}}\right) + \widehat{v}\left(\dfrac{\partial \widehat{u}}{\partial \widehat{y}}\right) = \dfrac{(\mu_{nf}+\kappa)}{\rho_{nf}}\left(\dfrac{\partial^2 \widehat{u}}{\partial \widehat{y}^2}\right) + \dfrac{\kappa}{\rho_{nf}}\left(\dfrac{\partial \widehat{N}}{\partial \widehat{y}}\right) + \dfrac{\pi j_0 M(\widehat{x})}{8\rho_{nf}} exp\left(-\dfrac{\pi}{a_0}\widehat{y}\right) \right\}, \\ BCs_{\widehat{(u,v)}} : \{\widehat{u}(\widehat{x}, \widehat{y}=0) = u_w(\widehat{x}) = s\widehat{x}\ ,\ v(\widehat{x}, \widehat{y}=0) = 0\ \&\ \widehat{u}(\widehat{x}, \widehat{y}\to\infty) \to 0\ \} \end{array} \right\}, \tag{1}$$

$$\left\{ \begin{array}{l} Eq_{\widehat{N}} : \left\{ j\rho_{nf}\left(\widehat{u}\dfrac{\partial \widehat{N}}{\partial \widehat{x}} + \widehat{v}\dfrac{\partial \widehat{N}}{\partial \widehat{y}}\right) = -\kappa\dfrac{\partial \widehat{u}}{\partial \widehat{y}} + j\left(\mu_{nf} + \dfrac{\kappa}{2}\right)\dfrac{\partial^2 \widehat{N}}{\partial \widehat{y}^2} - 2\kappa\widehat{N} \right\}, \\ BCs_{\widehat{N}} : \left\{ \left(\widehat{N} = -n\dfrac{\partial \widehat{u}}{\partial \widehat{y}}\right)_{(\widehat{x},\widehat{y}=0)}\ \&\ N(\widehat{x}, \widehat{y}\to\infty) \to 0 \right\} \end{array} \right\}, \tag{2}$$

$$\left\{ \begin{array}{l} Eq_{\widehat{T}} : \left\{ \widehat{u}\dfrac{\partial \widehat{T}}{\partial \widehat{x}} + \widehat{v}\dfrac{\partial \widehat{T}}{\partial \widehat{y}} = \left\{ \dfrac{k_{nf}}{(\rho C_P)_{nf}}\left(\dfrac{\partial^2 \widehat{T}}{\partial \widehat{y}^2}\right) + \dfrac{(\rho C_P)_{CuO} M_{CuO}\, D_B}{(\rho C_P)_{nf}\rho_{CuO}}\left(\dfrac{\partial \widehat{T}}{\partial \widehat{y}}\right)\left(\dfrac{\partial \widehat{C}}{\partial \widehat{y}}\right) + \right. \right. \\ \left. \left. \dfrac{(\rho C_P)_{CuO} D_T}{(\rho C_P)_{nf} T_\infty}\left(\dfrac{\partial \widehat{T}}{\partial \widehat{y}}\right)^2 + \dfrac{Q_E}{(\rho C_P)_{nf}} exp\left(-\delta\sqrt{\dfrac{a}{\upsilon_{hbf}}}\widehat{y}\right)(\widehat{T} - T_\infty) \right\} \right\}, \\ BCs_{\widehat{T}} : \left\{ \left[\dfrac{\partial \widehat{T}}{\partial \widehat{y}} = \dfrac{h_f}{k_{nf}}(\widehat{T} - T_f)\right]_{(\widehat{x},\widehat{y}=0)}\ \&\ \widehat{T}(\widehat{x}, \widehat{y}\to\infty) \to T_\infty \right\} \end{array} \right\}, \tag{3}$$

$$\left\{ \begin{array}{l} Eq_{\widehat{C}} : \left\{ \widehat{u}\left(\dfrac{\partial \widehat{C}}{\partial \widehat{x}}\right) + \widehat{v}\left(\dfrac{\partial \widehat{C}}{\partial \widehat{y}}\right) = D_B\left(\dfrac{\partial^2 \widehat{C}}{\partial \widehat{y}^2}\right) + \dfrac{\rho_{CuO}\, D_T}{M_{CuO} T_\infty}\left(\dfrac{\partial^2 \widehat{T}}{\partial \widehat{y}^2}\right) \right\}, \\ BCs_{\widehat{C}} : \left\{ \left(\dfrac{\partial \widehat{C}}{\partial \widehat{y}} = -\Lambda\dfrac{\partial \widehat{T}}{\partial \widehat{y}}\right)_{(\widehat{x},\widehat{y}=0)}\ \&\ \widehat{C}(\widehat{x}, \widehat{y}\to\infty) \to C_\infty \right\} \end{array} \right\}, \tag{4}$$

in which

$$\Lambda = \frac{\rho_{CuO} D_T}{M_{CuO} D_B T_\infty}. \tag{5}$$

Indeed, the proposed micropolar nanofluid flow model is derived appropriately based on the authenticated theoretical models and experimental correlations regrouped in Table 1 and Table 2, which permit to achieve realistically a better estimation of the thermal and other physical appearances describing the nanofluidic mixture $CuO - [(60\%) - C_2H_6O_2 + (40\%) - H_2O]$ at the temperature $T_0 = 300K$.

To reduce the mathematical complexity degree of the present nanofluid flow problem, the following similarity conversions are employed [54]:

Table 1
Thermophysical properties of each phase [50–52].

Properties	Hybrid base fluid $[(60\%) - C_2H_6O_2 + (40\%) - H_2O]$	Nanoparticles (CuO)
$\rho-$ Density	$\rho_{hbf} = -0.0024T_0^2 + 0.963T_0 + 1009.8$	$\rho_{CuO} = 6320\ kg\, m^{-3}$
$\mu-$ Dynamic viscosity	$\mu_{hbf} = 0.555 \times 10^{-6} exp\left(\frac{2664}{T_0}\right)$	
C_P- Specific heat	$(C_P)_{hbf} = 4.2483T_0 + 1882.4$	$(C_P)_{CuO} = 531.8j\ kg^{-1}K^{-1}$
$k-$ Thermal conductivity	$k_{hbf} = -3 \times 10^{-6}T_0^2 + 0.0025T_0 - 0.1057$	$k_{CuO} = 76.5\ Wm^{-1}K^{-1}$

Table 2
Thermophysical properties of the studied biphasic mixture [51–53].

Properties	Proposed models for $CuO-[(60\%)-C_2H_6O_2+(40\%)-H_2O]$
$\rho-$ Density	$\rho_{nf}=(1-\varphi_0)\rho_{hbf}+\varphi_0\rho_{CuO}$
$\mu-$ Dynamic viscosity	$\mu_{nf}=0.9197\mu_{hbf}exp(22.8539\varphi_0)$
$(\rho C_P)-$ Heat capacitance	$(\rho C_P)_{nf}=(1-\varphi_0)(\rho C_P)_{hbf}+\varphi_0(\rho C_P)_{CuO}$
$k-$ Thermal conductivity	$k_{nf}=k_s+5\times10^4\varphi_0(\rho C_P)_{hbf}\sqrt{\frac{k_BT_0}{\rho_{CuO}\,d_{CuO}}}f(T_0,\varphi_0)$
	$k_s=\left[1+\frac{3\varphi_0(k_{CuO}-k_{hbf})}{(k_{CuO}+2k_{hbf})-\varphi_0(k_{CuO}-k_{hbf})}\right]k_{hbf}$
	$f(T_0,\varphi_0)=\left(\frac{T_0}{T_{ref}}f_1-f_2\right)f_3$
	$f_1=2.8217\times10^{-2}\varphi_0+3.917\times10^{-3}$
	$f_2=3.0669\times10^{-2}\varphi_0+3.91123\times10^{-3}$
	$f_3=\frac{9.881}{(100\varphi_0)^{0.9446}}$

$$\left\{\begin{array}{l}\xi=\sqrt{\frac{s}{\upsilon_{hbf}}}\hat{x}\ ,\ \eta=\sqrt{\frac{s}{\upsilon_{hbf}}}\hat{y}\ ,\ \hat{u}(\hat{x},\hat{y})=u_w(\hat{x})f^{'}(\eta)\ ,\ \hat{v}(\hat{x},\hat{y})=-\sqrt{s\upsilon_{hbf}}f(\eta),\\ \widehat{N}(\hat{x},\hat{y})=\sqrt{\frac{s}{\upsilon_{hbf}}}u_w(\hat{x})g(\eta)\ ,\ \theta(\eta)=\frac{\widehat{T}(\hat{x},\hat{y})-T_\infty}{T_f-T_\infty}\ \&\ \chi(\eta)=\frac{\widehat{C}(\hat{x},\hat{y})-C_\infty}{C_\infty}\end{array}\right\}. \tag{6}$$

Accordingly, the governing boundary layer equations are transformed into the subsequent set of ODEs and BCs:

$$\left\{\begin{array}{l}Eq_f:\left\{\left(\frac{\mu_r+K}{\rho_r}\right)f^{'''}+\frac{K}{\rho_r}g^{'}+ff^{''}-f^{'2}+\frac{H}{\rho_r}exp(-\lambda\eta)=0\right\},\\ BCs_f:\{f(\eta=0)=0\ ,\ f^{'}(\eta=0)=1\ \&\ f^{'}(\eta=\eta_\infty)\to\ 0\}\end{array}\right\}, \tag{7}$$

$$\left\{\begin{array}{l}Eq_g:\left\{-\frac{\gamma K}{\rho_r}f^{''}+\left(\frac{2\mu_r+K}{2\rho_r}\right)g^{''}-\frac{2K\gamma}{\rho_r}g+\begin{vmatrix}f & g\\ f^{'} & g^{'}\end{vmatrix}=0\right\},\\ BCs_g:\{g(\eta=0)=-nf^{''}(\eta=0)\ \&\ g(\eta=\eta_\infty)\to\ 0\}\end{array}\right\}, \tag{8}$$

$$\left\{\begin{array}{l}Eq_\theta:\left\{\theta^{''}+\frac{(\rho C_P)_r\Pr}{k_r}f\theta^{'}+\frac{\Pr}{k_r}\begin{vmatrix}N_B\theta^{'} & -\theta^{'}\\ N_T\theta^{'} & \chi^{'}\end{vmatrix}+\frac{\Pr Q}{k_r}exp(-\delta\eta)\theta=0\right\},\\ BCs_\theta:\left\{\theta^{'}(0)=\frac{Bi}{k_r}[\theta(\eta=0)-1]\ \&\ \theta(\eta=\eta_\infty)\to0\right\}\end{array}\right\}, \tag{9}$$

$$\left\{\begin{array}{l}Eq_\chi:\left\{\frac{N_T}{N_B}\theta^{''}+\chi^{''}+Scf\chi^{'}=0\right\},\\ BCs_\chi:\left\{\chi^{'}(\eta=0)=-\frac{N_T}{N_B}\theta^{'}(\eta=0)\ \&\ \chi(\eta=\eta_\infty)\to0\right\}\end{array}\right\}. \tag{10}$$

As shown above, the indeterminate boundary $\eta_\infty\ (\eta\to\infty)$ refers to an estimated unitless value characterizing the boundary layer thicknesses assuring the asymptotical convergence of all solutions to the free-stream boundary conditions. In addition, the relative thermophysical properties $\{\rho_r,\mu_r,(\rho C_P)_r\&k_r\}$ that appeared in the dimensionless formulation are defined as:

$$\left\{\rho_r=\frac{\rho_{nf}}{\rho_{hbf}}\ ,\ \mu_r=\frac{\mu_{nf}}{\mu_{hbf}}\ ,\ (\rho C_P)_r=\frac{(\rho C_P)_{nf}}{(\rho C_P)_{hbf}}\ \&\ k_r=\frac{k_{nf}}{k_{hbf}}\right\}. \tag{11}$$

For more clarification, the embedded control parameters and their characteristics are enlisted in Table 3. However, the other quantities and abbreviations are provided in the nomenclature list.

In this investigation, the skin-friction factor $C_{f\hat{x}}$, the couple-stress coefficient $C_{n\hat{x}}$, the Nusselt number $Nu_{\hat{x}}$, the unitless wall temperature θ_w, and the reduced wall concentration C_w^* are among the main quantities of interest considered in this investigation, which are expressed as:

Table 3
A list of the relevant nanofluid flow parameters and their characteristics.

Parameters	Ranges	Default values
$Re_{\widehat{x}}\left[=\frac{s\widehat{x}^2}{\upsilon_{hbf}}\right]$ – Reynolds number	–	–
$\Pr\left[=\frac{\mu_{hbf}(C_P)_{hbf}}{k_{hbf}}\right]$ – Prandtl number	$\Pr = 33.64$	33.64
φ_0 – Inserted nanoparticles' volume fraction	$0.01 \le \varphi_0 \le 0.06$	0.01
n – Micro-gyration constraint	$0 \le n \le 1$	0.6
$K\left[=\frac{\kappa}{\mu_{hbf}}\right]$ – Micropolar parameter	$2 \le K \le 8$	2
$\gamma\left[=\frac{\upsilon_{hbf}}{js}\right]$ – Micro-inertial parameter	$\gamma = 1$	1
$\lambda\left[=\frac{\pi}{a_0}\sqrt{\frac{\upsilon_{hbf}}{s}}\right]$ – EMHD material parameter	$\lambda = 5$	5
$H\left[=\frac{\pi j_0 M_0}{8\rho_{hbf}s^2}\right]$ – Hartman number (Modified version)	$0 \le H \le 1.5$	0.5
δ – Exponentially decaying pre-factor	$\delta = 1$	1
$Q\left[=\frac{Q_E}{s(\rho C_P)_{hbf}}\right]$ – Heating source parameter	$0 \le Q \le 0.6$	0.2
$Bi\left[=\frac{h_f}{k_{hbf}}\sqrt{\frac{\upsilon_{hbf}}{s}}\right]$ – Thermal Biot number	$1 \le Bi \le 5$	5
$N_T\left[=\frac{(\rho C_P)_{CuO}D_T(T_f-T_\infty)}{(\rho C_P)_{hbf}\upsilon_{hbf}T_\infty}\right]$ – Thermophoresis parameter	$0.1 \le N_T \le 0.4$	0.1
$N_B\left[=\frac{(\rho C_P)_{CuO}D_B M_{CuO}C_\infty}{(\rho C_P)_{hbf}\rho_{CuO}\upsilon_{hbf}}\right]$ – Brownian motion parameter	$0.4 \le N_B \le 1$	0.8
$Sc\left[=\frac{\upsilon_{hbf}}{D_B}\right]$ – Schmidt number	$1 \le Sc \le 4$	1

$$\left\{\begin{array}{l} C_{f\widehat{x}} = \dfrac{\left[(\mu_{nf}+\kappa)\dfrac{\partial\widehat{u}}{\partial\widehat{y}}+\kappa\widehat{N}\right]_{\widehat{(x,y=0)}}}{\rho_{hbf}u_w^2(\widehat{x})}\ ,\ C_{n\widehat{x}} = \dfrac{\upsilon_{hbf}\left(\mu_{nf}+\dfrac{\kappa}{2}\right)j\left(\dfrac{\partial\widehat{N}}{\partial\widehat{y}}\right)_{\widehat{(x,y=0)}}}{\rho_{hbf}ju_w^3(\widehat{x})}, \\ Nu_{\widehat{x}} = \dfrac{-k_{nf}\widehat{x}\left(\dfrac{\partial\widehat{T}}{\partial\widehat{y}}\right)_{\widehat{(x,y=0)}}}{k_{hbf}\left(T_f-T_\infty\right)}\ ,\ \theta_w = \dfrac{\widehat{T}(\widehat{x},\widehat{y}=0)-T_\infty}{T_f-T_\infty}\ \&\ C_w^* = \dfrac{\widehat{C}(\widehat{x},\widehat{y}=0)}{C_\infty} \end{array}\right\}. \tag{12}$$

After simplifications, we get:

$$\left\{C_f = -[\mu_r + K(1-n)]f''(0)\ ,\ C_n = -\left(\frac{2\mu_r+K}{2}\right)g'(0)\ ,\ Nu = -k_r\theta'(0)\ ,\ \theta_w = \theta(0)\ \&\ C_w^* = \chi(0)+1\right\}. \tag{13}$$

Moreover, the reduced quantities $\{C_f, C_n\ \&\ Nu\}$ shown in Eq. (13) are defined as:

$$\left\{C_f = -\sqrt{Re_{\widehat{x}}}C_{f\widehat{x}}\ ,\ C_n = -Re_{\widehat{x}}C_{n\widehat{x}}\ \&\ Nu = \frac{Nu_{\widehat{x}}}{\sqrt{Re_{\widehat{x}}}}\right\}. \tag{14}$$

3. Methodology and authentication of results

Because of the nonlinearity specificity of the governing ODEs given by the coupled set of Eqs. 7–10, a robust hybrid GDQNRM

Table 4
Validation of GDQNRM results in the case where $\{H=0, Q=0\ \&\ Bi\to\infty\}$.

K	$\{\rho_r=\mu_r=\sigma_r=(\rho C_P)_r=k_r=1, \Pr=7, n=0.5, \gamma=1, N_T=0.4, N_B=0.8\ \&\ Sc=1.1\}$				
	Source	$-f''(0)$	$-g'(0)$	$-\theta'(0)$	$\chi'(0)$
1	Wakif et al. [44]	0.81649659	0.33333333	1.81001326	0.90500663
	Present results	0.8164965948	0.3333333333	1.8100132656	0.9050066328
2	Wakif et al. [44]	0.70710689	0.25000000	1.83475632	0.91737816
	Present results	0.7071068906	0.2500000000	1.8347563230	0.9173781615
3	Wakif et al. [44]	0.63245596	0.20000000	1.85158577	0.92579288
	Present results	0.6324559672	0.2000000000	1.8515857762	0.9257928881
4	Wakif et al. [44]	0.57735146	0.16666666	1.86397804	0.93198902
	Present results	0.5773514600	0.1666666666	1.8639780421	0.9319890210
5	Wakif et al. [44]	0.53452506	0.14285714	1.87359062	0.93679531
	Present results	0.5345250684	0.1428571428	1.8735906211	0.9367953105

algorithm [55–59] (i.e., generalized differential quadrature Newton-Raphson method) is developed properly to generate GDQNRM solutions discretely on the Chebyshev-Gauss-Lobatto collocation points [60,61], which should be involved in the computational domain $[0, \eta_\infty]$. For this purpose, several computational assessments are done with the help of Matlab software to generate the GDQNRM datasets for the dimensionless quantities $\{f'(\eta), g(\eta), \theta(\eta), \chi(\eta), C_f, C_n, Nu, \theta_w \ \& \ C_w^*\}$ as illustrated in Figs. 2–10 and Tables 4–9. Besides, the multiple comparisons performed in Tables 4 and 5 prove the validity of the executed GDQNRM code, whose quantitative results are found to be in a higher order of harmony with those published recently by Wakif et al. [44]. This agreement ascertains the robustness of the executed GDQNRM code and its numerical capability of providing faultless results for the present nanofluid flow problem.

By making use of the trapezoidal integration method, the involved square residual errors $\{\Delta f, \Delta g, \Delta\theta \& \Delta\chi\}$ are computed as follows:

$$\Delta f = \int_0^{\eta_\infty} \left\{ \left(\frac{\mu_r + K}{\rho_r}\right) f'''(\eta) + \frac{K}{\rho_r} g'(\eta) + f(\eta) f''(\eta) - f'^2(\eta) + \frac{H}{\rho_r} exp(-\lambda\eta) \right\}^2 d\eta, \tag{15}$$

$$\Delta g = \int_0^{\eta_\infty} \left\{ -\frac{\gamma K}{\rho_r} f''(\eta) + \left(\frac{2\mu_r + K}{2\rho_r}\right) g''(\eta) - \frac{2K\gamma}{\rho_r} g(\eta) + \begin{vmatrix} f(\eta) & g(\eta) \\ f'(\eta) & g'(\eta) \end{vmatrix} \right\}^2 d\eta, \tag{16}$$

$$\Delta\theta = \int_0^{\eta_\infty} \left\{ \theta''(\eta) + \frac{(\rho C_P)_r \mathrm{Pr}}{k_r} f(\eta)\theta'(\eta) + \frac{\mathrm{Pr}}{k_r} \begin{vmatrix} N_B\theta'(\eta) & -\theta'(\eta) \\ N_T\theta'(\eta) & \chi'(\eta) \end{vmatrix} + \frac{\mathrm{Pr}Q}{k_r} exp(-\delta\eta)\theta(\eta) \right\}^2 d\eta, \tag{17}$$

Table 5
Validation of GDQNRM results for Nu when $\{K = 0, \gamma = 0, H = 0, Q = 0 \ \& \ Bi \to \infty\}$.

N_T	$\{\rho_r = \mu_r = \sigma_r = (\rho C_P)_r = k_r = 1, N_B = 0.1 \ \& \ Sc = 10\}$		
	Source	Pr = 6.2	Pr = 14.2
0.1	Ishfaq et al. [62]	1.6198	2.4835
	Wakif et al. [44]	1.61980791	2.48355126
	Present results	1.6198079185	2.4835512644
0.2	Ishfaq et al. [62]	1.4749	2.1815
	Wakif et al. [44]	1.47492523	2.18148324
	Present results	1.4749252363	2.1814832490
0.3	Ishfaq et al. [62]	1.3381	1.8959
	Wakif et al. [44]	1.33812561	1.89589112
	Present results	1.338125615	1.8958911266
0.4	Ishfaq et al. [62]	1.2110	1.6371
	Wakif et al. [44]	1.21099539	1.63719091
	Present results	1.2109953930	1.6371909195
0.5	Ishfaq et al. [62]	1.0947	1.4126
	Wakif et al. [44]	1.09469797	1.41254319
	Present results	1.0946979758	1.4125431904

Table 6
GDQNRM estimation of Δf and Δg in different situations.

Parameters	Values	Δf	Δg
φ_0	0.010	2.96×10^{-21}	7.63×10^{-26}
	0.025	2.93×10^{-22}	4.82×10^{-26}
	0.045	1.42×10^{-20}	7.13×10^{-26}
	0.060	3.19×10^{-21}	1.37×10^{-26}
n	0.0	4.22×10^{-22}	5.32×10^{-26}
	0.3	7.26×10^{-23}	1.52×10^{-26}
	0.6	2.96×10^{-21}	7.63×10^{-26}
	0.9	6.02×10^{-22}	3.19×10^{-26}
K	2	2.96×10^{-21}	7.63×10^{-26}
	4	5.15×10^{-21}	4.36×10^{-25}
	6	2.71×10^{-20}	4.17×10^{-25}
	8	3.37×10^{-20}	1.41×10^{-24}
H	0.0	9.48×10^{-22}	6.77×10^{-26}
	0.5	2.96×10^{-21}	7.63×10^{-26}
	1.0	2.75×10^{-20}	4.86×10^{-25}
	1.5	3.93×10^{-21}	4.23×10^{-26}

Table 7
GDQNRM estimation of $\Delta\theta$ and $\Delta\chi$ in different situations.

Parameters	Values	$\Delta\theta$	$\Delta\chi$
φ_0	0.010	1.17×10^{-27}	5.24×10^{-29}
	0.025	3.84×10^{-27}	2.23×10^{-29}
	0.045	1.30×10^{-28}	1.84×10^{-28}
	0.060	1.08×10^{-28}	2.06×10^{-29}
H	0.0	9.10×10^{-27}	3.73×10^{-28}
	0.5	1.17×10^{-27}	5.24×10^{-29}
	1.0	1.06×10^{-27}	9.24×10^{-30}
	1.5	6.35×10^{-28}	6.80×10^{-31}
Q	0.0	6.04×10^{-28}	7.26×10^{-29}
	0.2	1.17×10^{-27}	5.24×10^{-29}
	0.4	1.60×10^{-26}	4.50×10^{-28}
	0.6	2.19×10^{-27}	6.56×10^{-28}
Bi	1	3.66×10^{-30}	7.06×10^{-31}
	2	2.76×10^{-29}	2.20×10^{-29}
	3	1.43×10^{-27}	2.03×10^{-28}
	5	1.17×10^{-27}	5.24×10^{-29}
N_T	0.1	1.17×10^{-27}	5.24×10^{-29}
	0.2	9.22×10^{-28}	1.28×10^{-28}
	0.3	7.26×10^{-27}	8.46×10^{-28}
N_B	0.4	3.46×10^{-27}	3.46×10^{-27}
	0.4	1.12×10^{-26}	6.14×10^{-30}
	0.6	7.11×10^{-28}	7.21×10^{-28}
	0.8	1.17×10^{-27}	5.24×10^{-29}
	1.0	8.44×10^{-28}	7.48×10^{-30}
Sc	1	1.17×10^{-27}	5.24×10^{-29}
	2	4.32×10^{-27}	5.74×10^{-29}
	3	1.89×10^{-27}	1.58×10^{-28}
	4	1.46×10^{-27}	2.28×10^{-30}

$$\Delta\chi = \int_0^{\eta_\infty} \left\{ \frac{N_T}{N_B}\theta''(\eta) + \chi''(\eta) + Scf(\eta)\chi'(\eta) \right\}^2 d\eta. \tag{18}$$

Technically, the convergence of the local results $\{f''(0), g'(0), \theta'(0) \,\&\, \chi'(0)\}$ is achieved once the absolute difference between two successive iterations satisfies the following criterion:

$$Max\left\{ \left|f''_{i+1}(0) - f''_i(0)\right|,\ \left|g'_{i+1}(0) - g'_i(0)\right|,\ \left|\theta'_{i+1}(0) - \theta'_i(0)\right|,\ \left|\chi'_{i+1}(0) - \chi'_i(0)\right| \right\} < 10^{-10}. \tag{19}$$

Quantitatively, the application of the above convergence condition leads to very low square residual errors as demonstrated in Tables 6 and 7, which confirm again the reliability of the presented numerical results. Computationally, it is more recommended to fix the infinite boundary condition at the value $\eta_\infty = 8$ along with seventy collocation points to attain the necessary GDQNRM accuracy.

4. Discussion of results

To reach the emphasized objectives successfully, several graphical illustrations and tabular demonstrations are provided in the ongoing section as displayed in Figs. 2–10, Table 8, and Table 9, in which conclusive physical explanations can be constructed for each observed occurrence by scrutinizing numerically the resulting micro-rotation motion of the existing micro-structures as well as the prominent thermal and mass features characterizing the transport phenomena that can be happened effectively during the steady convective flow of the micropolar nanofluid $CuO - [(60\%) - C_2H_6O_2 + (40\%) - H_2O]$ over a horizontal stretching Riga plate. Besides, these GDQNRM demonstrations are presented accordingly with a higher level of precision in terms of the unitless streamwise velocity function $f'(\eta)$, the dimensionless micro-rotation velocity function $g(\eta)$, the dimensionless temperature function $\theta(\eta)$, the dimensionless concentration function $\chi(\eta)$, the reduced skin-friction factor C_f, the reduced couple-stress coefficient C_n, the reduced Nusselt number Nu, the unitless wall temperature θ_w, and the rescaled wall concentration C_w^*. In this respect, the involved parameters $\{\varphi_0, n, K, H, Q, Bi, N_T, N_B \,\&\, Sc\}$ are adjusted in different scenarios in the vicinity of their default values highlighted in Table 3. However, the other flow parameters are kept constant at the values $\{\Pr = 33.64, \gamma = 1, \lambda = 5 \,\&\, \delta = 1\}$ during the present GDQNRM examination. According to Animasaun et al. [63], the demeanor of each embedded parameter and its impact degree on the reduced quantities $\{C_f, C_n, Nu, \theta_w \,\&\, C_w^*\}$ can be assessed statistically using the method of linear regression slope via Microsoft Excel software as exposed in Tables 8 and 9, in which the control parameter has an enhancing aspect on the evolution of an engineering quantity of interest when its corresponding linear regression slope is positive. Contrariwise, a declining consequence is depicted for the negative linear regression slopes.

The sways of the micro-gyration constraint n on the velocity profiles $\{f'(\eta) \,\&\, g(\eta)\}$ are delineated graphically in Fig.2 (a) and Fig.2 (b), respectively. As indicated in Fig. 2 (a), the progressing input of the parameter n dampers the streamwise velocity profile $f'(\eta)$,

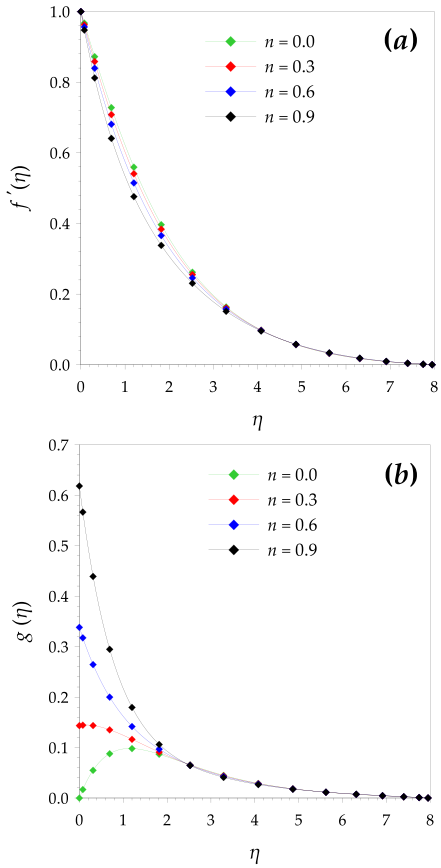

Fig. 2. Sway of n on $(a) - f'(\eta)$ and $(b) - g(\eta)$.

whereas an opposite impact is noticed in the case of the micro-rotation velocity profile $g(\eta)$. As mentioned previously, this control parameter reflects the nature of the rotating motion of the existing micro-elements at the electromagnetic surface. It is worth mentioning here that the value $n = 0$ corresponds to the case of a strong concentration of micro-elements, in which the micro-elements are incapable to revolve at the wall. Indeed, the micro-rotation motion of the existing micro-structures has an unfavorable influence on the dynamics of the micropolar nanofluidic medium. In this situation, the streamwise nanofluid velocity varies decreasingly with the micro-gyration parameter n. However, the micro-rotation velocity of micro-elements can be boosted by diminishing their concentration via the higher estimation in the parameter n. In addition, Fig.3 (a) and Fig.3 (b) are plotted to examine the effects of the micropolar parameter K on the dimensionless velocity functions $\{f'(\eta)\ \&\ g(\eta)\}$. It can be understood from Fig. 3 (a) that the streamwise velocity profile $f'(\eta)$ is advanced everywhere in the momentum boundary layer region with the growing values of the micropolar parameter K. This observation indicates obviously that the effective vortex viscosity of the micropolar nanofluid $CuO-[(60\%) - C_2H_6O_2 + (40\%) - H_2O]$ leads to a hastening impact on the nanofluid motion due to the induced micro-rotational inertial moments. On the contrary, a dual behavior is seen in Fig. 3 (b) for the micro-rotation velocity profile $g(\eta)$ when the micropolar parameter K is upsurged gradually. As a result, it is perceived that the micro-rotation velocity profile $g(\eta)$ declines noticeably near the Riga plate with the increase in the micropolar parameter K. This fact can be explained by the weakening in the micro-motion phenomenon that can be happened near the Riga plate. Whilst, a reverse tendency is observed away from the Riga plate. In a particular physical scenario, Fig.4 (a) and Fig.4 (b) prove that the streamwise velocity and micro-rotation velocity functions $\{f'(\eta)\ \&\ g(\eta)\}$ exhibit the same aspects towards the strengthening values of the modified Hartman number H like these sketched previously in Fig.3 (a) and Fig.3 (b) for the micropolar parameter K. It is important to clarify here that the sense of the fashioned Lorentz forces are adjusted practically in the Riga plate through the induced electrical current in such a way that the induced electromagnetic forces support the nanofluid motion. In this situation, the intensifying values of the electromagnetic parameter H deteriorate considerably the occurrence of micro-motion near the Riga plate.

Sequel to the afore-mentioned dynamical results, it is found that the electromagnetic parameter H shows a slightly declining trend against the temperature and concentration distributions $\{\theta(\eta)\ \&\ \chi(\eta)\}$ as revealed in Fig.5 (a) and Fig.5 (b). Mechanically, the induced Lorentz forces exhibit a higher strength when these electromagnetic actions are evaluated at the Riga plate. Keeping in mind the driven impact of the electromagnetic parameter H, the Lorentz forces will strongly hinder the thermal transmission between the convectively heated Riga plate and the surrounding nanofluidic medium by hastening superficially the nanofluid motion. For this reason, the

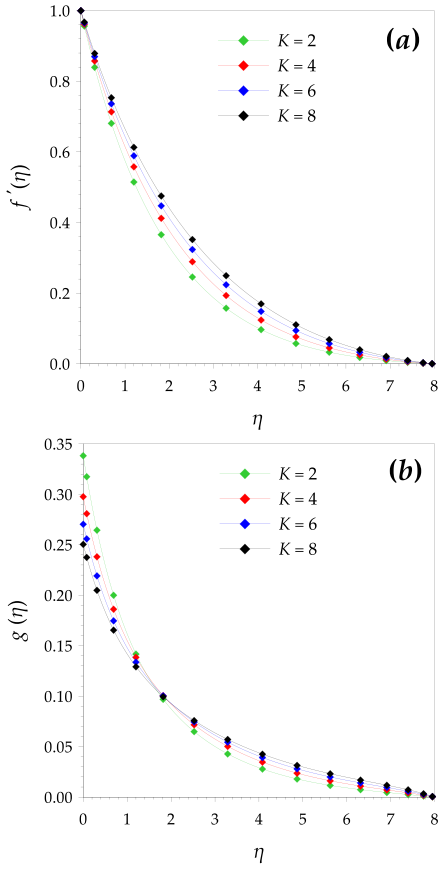

Fig. 3. Sway of K on $(a) - f'(\eta)$ and $(b) - g(\eta)$.

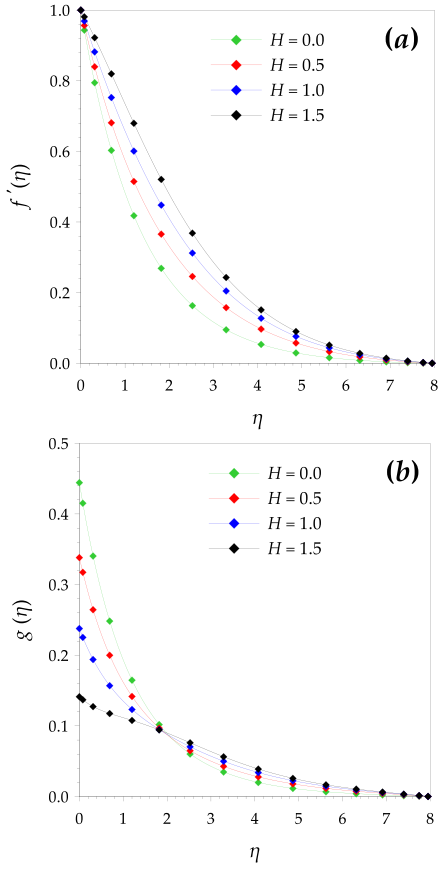

Fig. 4. Sway of H on $(a) - f'(\eta)$ and $(b) - g(\eta)$.

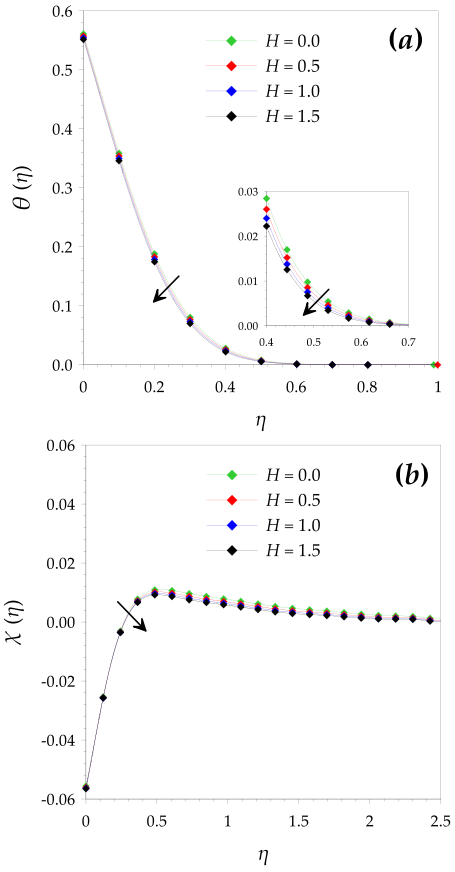

Fig. 5. Evolutions of $(a) - \theta(\eta)$ and $(b) - \chi(\eta)$ with the increase in the parameter H.

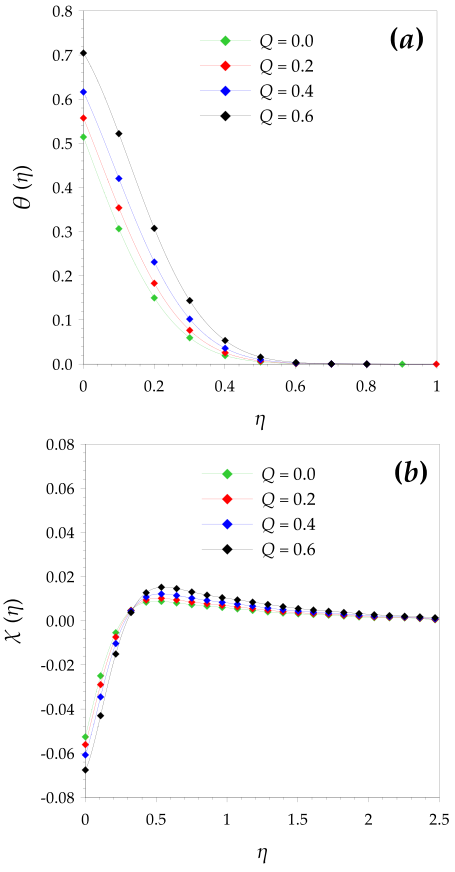

Fig. 6. Evolutions of $(a) - \theta(\eta)$ and $(b) - \chi(\eta)$ with the increase in the parameter Q.

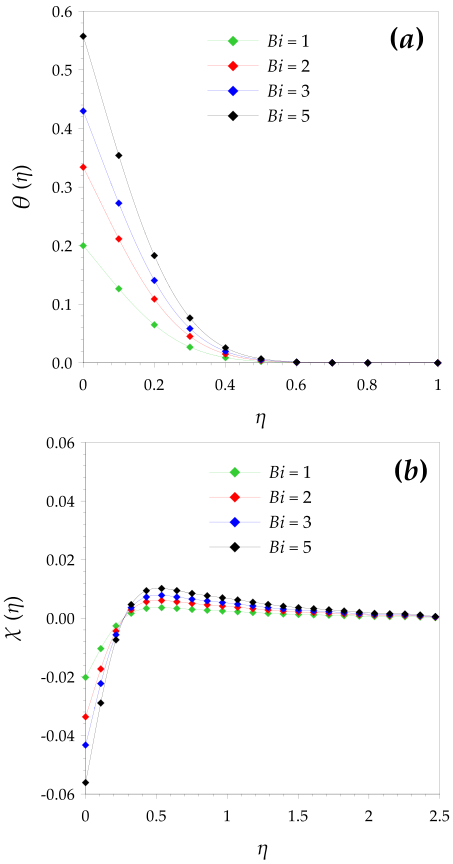

Fig. 7. Evolutions of $(a) - \theta(\eta)$ and $(b) - \chi(\eta)$ with the increase in the parameter *Bi*.

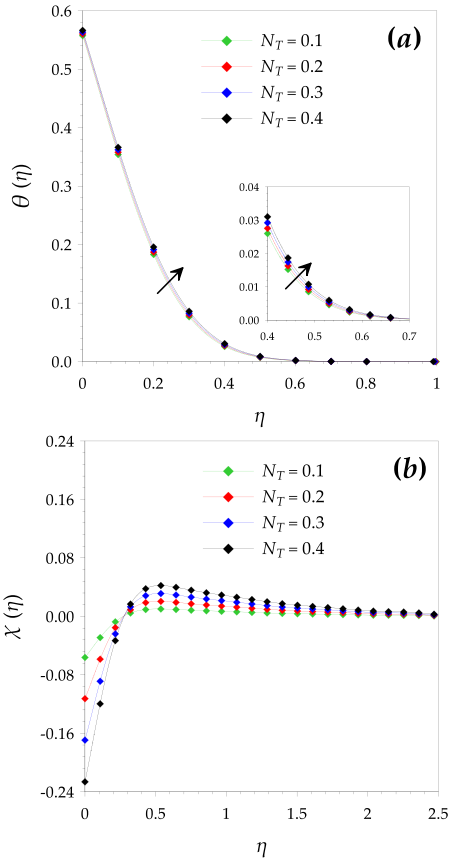

Fig. 8. Evolutions of $(a) - \theta(\eta)$ and $(b) - \chi(\eta)$ with the increase in the parameter N_T.

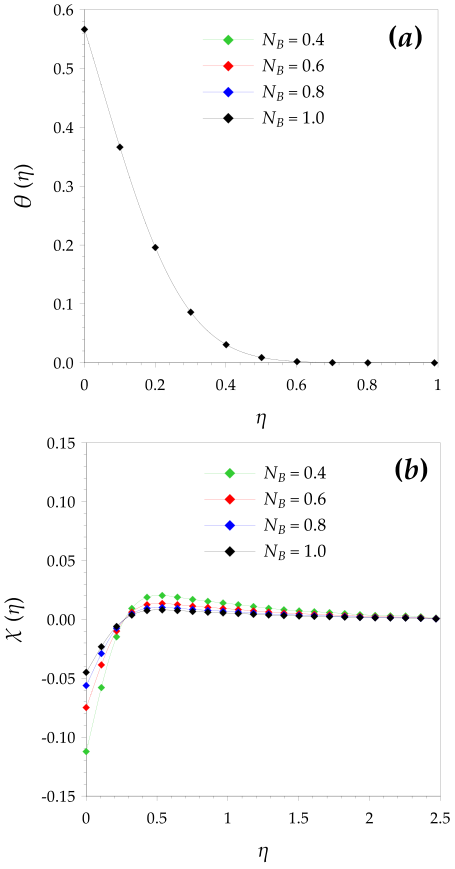

Fig. 9. Evolutions of $(a) - \theta(\eta)$ and $(b) - \chi(\eta)$ with the increase in the parameter N_B.

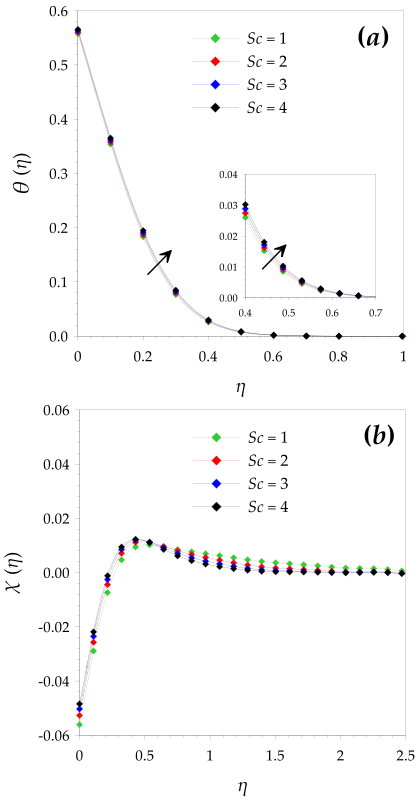

Fig. 10. Evolutions of $(a)-\theta(\eta)$ and $(b)-\chi(\eta)$ with the increase in the parameter Sc.

temperature distribution $\theta(\eta)$ gets dropped throughout the thermal boundary layer region. As a result of this cooling effect, a certain number of nanoparticles migrate from the concentration boundary layer region to the free-stream region, which leads to diminishment in the concentration distribution $\chi(\eta)$ with a thinning in its corresponding boundary layer region. An important thermal enhancement is viewed in Fig. 6 (a) for the temperature distribution $\theta(\eta)$ in response to the continuous increment in the magnitude of the heating source parameter Q. This thermal improvement can be explicated by the extra amount of thermal energy supplied internally within the nanofluidic medium by the variable heat source. Besides, the curves of Fig. 6 (b) demonstrate that the concentration distribution $\chi(\eta)$ shows a double aspect towards the higher values of the heating source parameter Q due to the partial migration of nanoparticles from

Table 8
Accurate values of C_f and C_n in different situations.

Parameters	Values	C_f	C_n
φ_0	0.010	1.1028266729	0.5910191917
	0.025	1.3069656817	0.6383362830
	0.045	1.6624657893	0.7023942713
	0.060	2.0092993734	0.7519111298
Linear regression slopes		**18,0805645438**	**3,2157781624**
n	0.0	1.3127481476	−0.4947394236
	0.3	1.2232613405	−0.0325405054
	0.6	1.1028266729	0.5910191917
	0.9	0.9316589158	1.4810508277
Linear regression slopes		**−0.4212341210**	**2.1836434837**
K	2	1.1028266729	0.5910191917
	4	1.3674858638	0.7003390963
	6	1.6028206952	0.7951051122
	8	1.8186505062	0.8801173006
Linear regression slopes		**0.1191403166**	**0.0481030171**
H	0.0	1.4486517774	0.8251534355
	0.5	1.1028266729	0.5910191917
	1.0	0.7755594134	0.3587122317
	1.5	0.4609737738	0.1273756422
Linear regression slopes		**−0.6580602541**	**−0.4651280680**

Table 9
Accurate values of Nu, θ_w, and C_w^* in different situations.

Parameters	Values	Nu	θ_w	C_w^*
φ_0	0.010	2.2124432352	0.5575113529	0.9438815984
	0.025	2.2414892721	0.5517021455	0.9446338060
	0.045	2.2794619108	0.5441076178	0.9455441709
	0.060	2.3079511276	0.5384097744	0.9461904428
Linear regression slopes		**1.9085680669**	**−0.3817136134**	**0.0460860407**
H	0.0	2.1952724825	0.5609455034	0.9443688397
	0.5	2.2124432352	0.5575113529	0.9438815984
	1.0	2.2277363761	0.5544527247	0.9436223384
	1.5	2.2416850998	0.5516629800	0.9434764770
Linear regression slopes		**0.0309061986**	**−0.0061812397**	**−0.0005872696**
Q	0.0	2.4275253635	0.5144949272	0.9474362655
	0.2	2.2124432352	0.5575113529	0.9438815984
	0.4	1.9177863247	0.6164427350	0.9391116205
	0.6	1.4771610921	0.7045677815	0.9321430248
Linear regression slopes		**−1.5728748624**	**0.3145749725**	**−0.0253248500**
Bi	1	0.7999015388	0.2000984611	0.9798311489
	2	1.3318468009	0.3340765995	0.9663437941
	3	1.7103888408	0.4298703863	0.9567088034
	5	2.2124432352	0.5575113529	0.9438815984
Linear regression slopes		**0.3436436224**	**0.0869872439**	**−0.0087487496**
N_T	0.1	2.2124432352	0.5575113529	0.9438815984
	0.2	2.1979752129	0.5604049574	0.8874261976
	0.3	2.1830259873	0.5633948025	0.8306234533
	0.4	2.1675635912	0.5664872817	0.7734625435
Linear regression slopes		**−0.1495881576**	**0.0299176315**	**−0.5680599090**
N_B	0.4	2.2124432352	0.5575113529	0.8877631968
	0.6	2.2124432352	0.5575113529	0.9251754645
	0.8	2.2124432352	0.5575113529	0.9438815984
	1.0	2.2124432352	0.5575113529	0.9551052787
Linear regression slopes		**0.0000000000**	**0.0000000000**	**0.1103661898**
Sc	1	2.2124432352	0.5575113529	0.9438815984
	2	2.1985987907	0.5602802418	0.9472762494
	3	2.1849384822	0.5630123035	0.9496500042
	4	2.1714720123	0.5657055975	0.9515104766
Linear regression slopes		**−0.0136573977**	**0.0027314796**	**0.0025260389**

the heated Riga plate to the cold region to reach the top-heavy configuration. Due to the minimization in the thermal resistance at the fluid-solid interface, the temperature distribution $\theta(\eta)$ increases with the augmenting values of the thermal Biot number Bi as underlined graphically in Fig. 7 (a). This thermal amelioration constitutes a fundamental energetical source for the nanoparticles to move from the hot region to the cold one as pointed out in Fig. 7 (b). Similarly, the results of Fig.8 (a) and Fig.8 (b) ascertain that the upward thermo-migration of nanoparticles from the heated surface to the cold zone heightens somewhat the temperature of the nanofluidic medium due to the intensification in the thermophoresis diffusive process through the higher values of the nanofluid parameter N_T. On the contrary, it is demonstrated from Fig.9 (a) and Fig.9 (b) that the nanofluid temperature is unaffected by the downward nanoparticles' migration from the cold region to the hot zone (i.e., Brownian diffusive mechanism) when the Brownian motion parameter N_B is significant. Furthermore, Fig.10 (a) and Fig.10 (b) attest undoubtedly that the enormous values of the Schmidt number tend to increase sensitively the nanofluid temperature and suppress the concentration boundary layer region by regularizing the nanoparticles' distribution throughout the nanofluidic medium.

5. Concluding remarks

In the light of the afore numerical deliberation, the following GDQNRM results can be abbreviated:

- The parameter n shows a favorable impact on the micro-rotation velocity profile, whereas a slowing trend is depicted in the streamwise velocity profile.
- The parameter K exhibits a boosting tendency towards the streamwise velocity profile, whilst, a dual aspect is revealed in the micro-rotation velocity profile.
- The greater values of the electromagnetic parameter H accelerate the nanofluid motion, delay the manifestation of the rotational motion of micro-elements near the Riga plate, drop the nanofluid temperature, and diminish the nanoparticles' molar concentration distribution.
- The nanofluid temperature can be elevated by strengthening the thermophoresis mechanism via the larger values of the parameters $\{Q, Bi \,\&\, N_T\}$.
- A slight increase in the nanofluid temperature can be obtained by uniformizing the nanoparticles' distribution through the higher values of the parameter Sc, whereas the temperature profile remains unchanged by the increase in the parameter N_B.

- The magnitude of the frictional drag factor C_f can be weakened significantly either by lessening the parameters $\{\varphi_0 \ \& \ K\}$ or by amplifying the parameters $\{n \ \& \ H\}$.
- The couple-stress coefficient C_n can be improved effectively either by augmenting the parameters $\{\varphi_0, n \ \& \ K\}$ or by diminishing the parameter H.
- The wall heat transfer rate Nu can be ameliorated considerably either by heightening the parameters $\{\varphi_0, H \ \& \ Bi\}$ or by declining the parameters $\{Q, N_T \ \& \ Sc\}$, whereas the reduced thermal quantity Nu remains uninfluenced by the incrementing values given to the parameter N_B.
- The dimensionless wall temperature θ_w is a decreasing function of the parameters $\{\varphi_0 \ \& \ H\}$ and an increasing function of the parameters $\{Q, Bi, N_T \ \& \ Sc\}$, whilst this unitless local temperature is unaffected by the parameter N_B.
- An upsurge in the rescaled wall concentration C_w^* can be achieved successfully via the advanced values of the parameters $\{\varphi_0, N_B \ \& \ Sc\}$ or through the lower values of the parameters $\{H, Q, Bi \ \& \ N_T\}$

Credit author statement

The corresponding author "Prof. Se-Jin Yook" would like to mention that all the co-authors mentioned in this paper have directly contributed to the planning, correction, execution, and analysis of this innovative research work.

Declaration of competing interest

The authors declare that they have no known competing financial interests or personal relationships that could have appeared to influence the work reported in this paper.

Acknowledgments

This work was conducted under the Technology Innovation Program (or Industrial Strategic Technology Development Program - material part package type) as " Development of fire suppression-type high safety module and demonstration of safety for future eco-friendly medium and large secondary battery (No. 20015986) ", funded by the Ministry of Trade, Industry & Energy (MOTIE), Republic of Korea.

References

[1] J. Buongiorno, et al., A benchmark study on the thermal conductivity of nanofluids, J. Appl. Phys. 106 (2009), 94312, https://doi.org/10.1063/1.3245330.
[2] W. Yu, H. Xie, A review on nanofluids: preparation, stability mechanisms, and applications, J. Nanomater. 2012 (2012) 17, https://doi.org/10.1155/2012/435873. ID 435873.
[3] S.A. Angayarkanni, J. Philip, Review on thermal properties of nanofluids : recent developments, Adv. Colloid Interface Sci. 225 (2015) 146–176, https://doi.org/10.1016/j.cis.2015.08.014.
[4] K. Bashirnezhad, S. Bazri, M.R. Safaei, M. Goodarzi, M. Dahari, O. Mahian, A.S. Dalkılıça, S. Wongwises, Viscosity of nanofluids: a review of recent experimental studies, Int. Commun. Heat Mass Tran. 73 (2016) 114–123, https://doi.org/10.1016/j.icheatmasstransfer.2016.02.005.
[5] N.A.C. Sidik, S. Samion, J. Ghaderian, M.N.A.W.M. Yazid, Recent progress on the application of nanofluids in minimum quantity lubrication machining: a review, Int. J. Heat Mass Tran. 108 (2017) 79–89, https://doi.org/10.1016/j.ijheatmasstransfer.2016.11.105.
[6] A.I. Khan, A. Valan Arasu, A review of influence of nanoparticle synthesis and geometrical parameters on thermophysical properties and stability of nanofluids, Therm. Sci. Eng. Prog. 11 (2019) 334–364, https://doi.org/10.1016/j.tsep.2019.04.010.
[7] M.H. Esfe, M. Afrand, An updated review on the nanofluids characteristics, J. Therm. Anal. Calorim. 138 (2019) 4091–4101, https://doi.org/10.1007/s10973-019-08406-2.
[8] S.U.S. Choi, Enhancing Thermal Conductivity of Fluids with Nanoparticles, vol. 66, ASME, New York, 1995, pp. 99–105.
[9] N. Bozorgan, M. Shafahi, Performance evaluation of nanofluids in solar energy: a review of the recent literature, Micro Nano Syst. Lett. 3 (2015) 1–15, https://doi.org/10.1186/s40486-015-0014-2.
[10] W.H. Azmi, K.V. Sharma, R. Mamat, G. Najafi, M.S. Mohamad, The enhancement of effective thermal conductivity and effective dynamic viscosity of nanofluids-a review, Renew. Sustain. Energy Rev. 53 (2016) 1046–1058, https://doi.org/10.1016/j.rser.2015.09.081.
[11] M. Raja, R. Vijayan, P. Dineshkumar, M. Venkatesan, Review on nanofluids characterization, heat transfer characteristics and applications, Renew. Sustain. Energy Rev. 64 (2016) 163–173, https://doi.org/10.1016/j.rser.2016.05.079.
[12] N. Abbas, M.B. Awan, M. Amer, S.M. Ammar, U. Sajjad, H.M. Ali, N. Zahra, M. Hussain, M.A. Badshah, A.T. Jafry, Applications of nanofluids in photovoltaic thermal systems: a review of recent advances, Phys. A Stat. Mech. Appl. 536 (2019), 122513, https://doi.org/10.1016/j.physa.2019.122513.
[13] M. Ghalandari, A. Maleki, A. Haghighi, M. Safdari Shadloo, M. Alhuyi Nazari, I. Tlili, Applications of nanofluids containing carbon nanotubes in solar energy systems: a review, J. Mol. Liq. 313 (2020), 113476, https://doi.org/10.1016/j.molliq.2020.113476.
[14] N. Acharya, Framing the impacts of highly oscillating magnetic field on the ferrofluid flow over a spinning disk considering nanoparticle diameter and solid-liquid interfacial layer, J. Heat Tran. 142 (2020), 102503, https://doi.org/10.1115/1.4047503.
[15] N. Acharya, H. Mondal, P.K. Kundu, Spectral approach to study the entropy generation of radiative mixed convective couple stress fluid flow over a permeable stretching cylinder, Proc. Inst. Mech. Eng. Part C J. Mech. Eng. Sci. 235 (2020) 1–13, https://doi.org/10.1177/0954406220954893.
[16] N. Acharya, S. Maity, P.K. Kundu, Influence of inclined magnetic field on the flow of condensed nanomaterial over a slippery surface: the hybrid visualization, Appl. Nanosci. 10 (2020) 633–647, https://doi.org/10.1007/s13204-019-01123-0.
[17] N. Acharya, R. Bag, P.K. Kundu, On the impact of nonlinear thermal radiation on magnetized hybrid condensed nanofluid flow over a permeable texture, Appl. Nanosci. 10 (2020) 1679–1691, https://doi.org/10.1007/s13204-019-01224-w.
[18] N. Acharya, R. Bag, P.K. Kundu, On the mixed convective carbon nanotube flow over a convectively heated curved surface, Heat Transf. 49 (2020) 1713–1735, https://doi.org/10.1002/htj.21687.
[19] N. Acharya, Spectral quasi linearization simulation of radiative nanofluidic transport over a bended surface considering the effects of multiple convective conditions, Eur. J. Mech. B Fluid 84 (2020) 139–154, https://doi.org/10.1016/j.euromechflu.2020.06.004.
[20] N. Acharya, F. Mabood, On the hydrothermal features of radiative Fe3O4-graphene hybrid nanofluid flow over a slippery bended surface with heat source/sink, J. Therm. Anal. Calorim. 143 (2021) 1273–1289, https://doi.org/10.1007/s10973-020-09850-1.
[21] N. Acharya, Spectral quasi linearization simulation on the hydrothermal behavior of hybrid nanofluid spraying on an inclined spinning disk, Partial Differ. Equat. Appl. Math. 4 (2021), 100094, https://doi.org/10.1016/j.padiff.2021.100094.

[22] N. Acharya, Spectral quasi linearization simulation on the radiative nanofluid spraying over a permeable inclined spinning disk considering the existence of heat source/sink, Appl. Math. Comput. 411 (2021), 126547, https://doi.org/10.1016/j.amc.2021.126547.

[23] N. Acharya, A.J. Chamkha, On the magnetohydrodynamic Al2O3-water nanofluid flow through parallel fins enclosed inside a partially heated hexagonal cavity, Int. Commun. Heat Mass Tran. 132 (2022), 105885, https://doi.org/10.1016/j.icheatmasstransfer.2022.105885.

[24] N. Acharya, Impacts of different thermal modes of multiple obstacles on the hydrothermal analysis of Fe3O4-water nanofluid enclosed inside a nonuniformly heated cavity, Heat Transf. 51 (2022) 1376–1405, https://doi.org/10.1002/htj.22356.

[25] N. Acharya, Effects of different thermal modes of obstacles on the natural convective Al2O3-water nanofluidic transport inside a triangular cavity, Proc. Inst. Mech. Eng. Part C J. Mech. Eng. Sci. January (2022), 09544062211061484, https://doi.org/10.1177/09544062211061484.

[26] N. Acharya, Finite element analysis on the hydrothermal pattern of radiative natural convective nanofluid flow inside a square enclosure having nonuniform heated walls, Heat Transf. 51 (2022) 323–354, https://doi.org/10.1002/htj.22309.

[27] G. Rasool, A. Shafiq, S. Hussain, M. Zaydan, A. Wakif, A.J. Chamkha, M.S. Bhutta, Significance of Rosseland's radiative process on reactive Maxwell nanofluid flows over an isothermally heated stretching sheet in the presence of Darcy-Forchheimer and Lorentz forces: towards a new perspective on Buongiorno's model, Micromachines 13 (2022) 368, https://doi.org/10.3390/mi13030368.

[28] J. Buongiorno, Convective transport in nanofluids, J. Heat Tran. 128 (2006) 240–250, https://doi.org/10.1115/1.2150834.

[29] A. Dawar, A. Wakif, A. Saeed, Z. Shah, T. Muhammad, P. Kumam, Significance of Lorentz forces on Jeffrey nanofluid flows over a convectively heated flat surface featured by multiple velocity slips and dual stretching constraint: a homotopy analysis approach, J. Comput. Des. Eng. 9 (2022) 564–582, https://doi.org/10.1093/jcde/qwac019.

[30] N.A. Shah, A. Wakif, E.R. El-Zahar, T. Thumma, S.-J. Yook, Heat transfers thermodynamic activity of a second-grade ternary nanofluid flow over a vertical plate with Atangana-Baleanu time-fractional integral, Alex. Eng. J. 61 (2022) 10045–10053, https://doi.org/10.1016/j.aej.2022.03.048.

[31] R.K. Tiwari, M.K. Das, Heat transfer augmentation in a two-sided lid-driven differentially heated square cavity utilizing nanofluids, Int. J. Heat Mass Tran. 50 (2007) 2002–2018, https://doi.org/10.1016/j.ijheatmasstransfer.2006.09.034.

[32] A. Gailitis, On the possibility to reduce the hydrodynamic drag of a plate in an electrolyte, Appl. Magnetohydrodyn. Rep. Inst. Phys. Riga. 13 (1961) 143–146.

[33] A. Wakif, A. Chamkha, I.L. Animasaun, M. Zaydan, H. Waqas, R. Sehaqui, Novel physical insights into the thermodynamic irreversibilities within dissipative EMHD fluid flows past over a moving horizontal Riga plate in the coexistence of wall suction and Joule heating effects: a comprehensive numerical investigation, Arabian J. Sci. Eng. 45 (2020) 9423–9438, https://doi.org/10.1007/s13369-020-04757-3.

[34] R. Kumar, S. Sood, S.A. Shehzad, M. Sheikholeslami, Radiative heat transfer study for flow of non-Newtonian nanofluid past a Riga plate with variable thickness, J. Mol. Liq. 248 (2017) 143–152, https://doi.org/10.1016/j.molliq.2017.10.018.

[35] V.B. Awati, N. Mahesh Kumar, A. Wakif, Haar wavelet scrutinization of heat and mass transfer features during the convective boundary layer flow of a nanofluid moving over a nonlinearly stretching sheet, Partial Differ. Equat. Appl. Math. 4 (2021), 100192, https://doi.org/10.1016/j.padiff.2021.100192.

[36] P. Rana, R. Bhargava, Flow and heat transfer of a nanofluid over a nonlinearly stretching sheet: a numerical study, Commun. Nonlinear Sci. Numer. Simulat. 17 (2012) 212–226, https://doi.org/10.1016/j.cnsns.2011.05.009.

[37] A. Wakif, I.L. Animasaun, P.V. Satya Narayana, G. Sarojamma, Meta-analysis on thermo-migration of tiny/nano-sized particles in the motion of various fluids, Chin. J. Phys. 68 (2020) 293–307, https://doi.org/10.1016/j.cjph.2019.12.002.

[38] A. Zaib, R.U. Haq, A.J. Chamkha, M.M. Rashidi, Impact of partial slip on mixed convective flow towards a Riga plate comprising micropolar TiO2-kerosene/water nanoparticles, Int. J. Numer. Methods Heat Fluid Flow 29 (2019) 1647–1662, https://doi.org/10.1108/HFF-06-2018-0258.

[39] A. Naseem, A. Shafiq, L. Zhao, M.U. Farooq, Analytical investigation of third grade nanofluidic flow over a riga plate using Cattaneo-Christov model, Results Phys. 9 (2018) 961–969, https://doi.org/10.1016/j.rinp.2018.01.013.

[40] M.T. Akolade, Y.O. Tijani, A comparative study of three dimensional flow of Casson-Williamson nanofluids past a Riga plate:Spectral quasi-linearization approach, Partial Differ. Equat. Appl. Math. 4 (2021), 100108, https://doi.org/10.1016/j.padiff.2021.100108.

[41] G. Rasool, A. Wakif, Numerical spectral examination of EMHD mixed convective flow of second-grade nanofluid towards a vertical Riga plate using an advanced version of the revised Buongiorno's nanofluid model, J. Therm. Anal. Calorim. 143 (2021) 2379–2393, https://doi.org/10.1007/s10973-020-09865-8.

[42] K. Gangadhar, M.A. Kumari, A.J. Chamkha, EMHD flow of radiative second-grade nanofluid over a Riga plate due to convective heating: revised Buongiorno's nanofluid model, Arabian J. Sci. Eng. (2021) 1–11, https://doi.org/10.1007/s13369-021-06092-7.

[43] H. Vaidya, K.V. Prasad, I. Tlili, O.D. Makinde, C. Rajashekhar, S.U. Khan, R. Kumar, D.L. Mahendra, Mixed convective nanofluid flow over a non linearly stretched Riga plate, Case Stud. Therm. Eng. 24 (2021), 100828, https://doi.org/10.1016/j.csite.2020.100828.

[44] A. Wakif, M. Zaydan, A.S. Alshomrani, T. Muhammad, R. Sehaqui, New insights into the dynamics of alumina-(60% ethylene glycol + 40% water) over an isothermal stretching sheet using a renovated Buongiorno's approach: a numerical GDQLLM analysis, Int. Commun. Heat Mass Tran. 133 (2022), 105937, https://doi.org/10.1016/j.icheatmasstransfer.2022.105937.

[45] D.A. Nield, A.V. Kuznetsov, Thermal instability in a porous medium layer saturated by a nanofluid: a revised model, Int. J. Heat Mass Tran. 68 (2014) 211–214, https://doi.org/10.1016/j.ijheatmasstransfer.2013.09.026.

[46] D.A. Nield, A.V. Kuznetsov, The onset of convection in a horizontal nanofluid layer of finite depth : a revised model, Int. J. Heat Mass Tran. 77 (2014) 915–918, https://doi.org/10.1016/j.ijheatmasstransfer.2014.06.020.

[47] A. Wakif, I.L. Animasaun, U. Khan, N.A. Shah, T. Thumma, Dynamics of radiative-reactive Walters-B fluid due to mixed convection conveying gyrotactic microorganisms, tiny particles experience haphazard motion, thermo-migration, and Lorentz force, Phys. Scripta 96 (2021), 125239, https://doi.org/10.1088/1402-4896/ac2b4b.

[48] G. Lukaszewicz, Micropolar Fluids: Theory and Applications, Birkhäuser Basel, Springer Science and Business Media, New York, 1999, https://doi.org/10.1007/978-1-4612-0641-5.

[49] H. Schlichting, K. Gersten, Boundary-layer Theory, Springer, Berlin, Heidelberg, 2017, https://doi.org/10.1007/978-3-662-52919-5.

[50] K. Anantha Kumar, V. Sugunamma, N. Sandeep, Influence of viscous dissipation on MHD flow of micropolar fluid over a slendering stretching surface with modified heat flux model, J. Therm. Anal. Calorim. 139 (2020) 3661–3674, https://doi.org/10.1007/s10973-019-08694-8.

[51] ASHRAE Handbook, Fundamentals, American Society of Heating, Refrigeration and Air Conditioning Engineers, Inc., Atlanta, GA, 2005.

[52] R.S. Vajjha, D.K. Das, D.P. Kulkarni, Development of new correlations for convective heat transfer and friction factor in turbulent regime for nanofluids, Int. J. Heat Mass Tran. 53 (2010) 4607–4618, https://doi.org/10.1016/j.ijheatmasstransfer.2010.06.032.

[53] A. Wakif, R. Sehaqui, Generalized differential quadrature scrutinization of an advanced MHD stability problem concerned water-based nanofluids with metal/metal oxide nanomaterials: a proper application of the revised two-phase nanofluid model with convective heating and through-flow boundary conditions, Numer. Methods Part. Differ. Equ. 38 (2022) 608–635, https://doi.org/10.1002/num.22671.

[54] A. Dawar, Z. Shah, A. Tassaddiq, S. Islam, P. Kumam, Joule heating in magnetohydrodynamic micropolar boundary layer flow past a stretching sheet with chemical reaction and microstructural slip, Case Stud. Therm. Eng. 25 (2021), 100870, https://doi.org/10.1016/j.csite.2021.100870.

[55] C. Shu, Differential Quadrature and its Application in Engineering, Springer Science & Business Media, 2012.

[56] W.-F. Xia, I.L. Animasaun, A. Wakif, N.A. Shah, S.-J. Yook, Gear-generalized differential quadrature analysis of oscillatory convective Taylor-Couette flows of second-grade fluids subject to Lorentz and Darcy-Forchheimer quadratic drag forces, Int. Commun. Heat Mass Tran. 126 (2021), 105395, https://doi.org/10.1016/j.icheatmasstransfer.2021.105395.

[57] A.S. Sabu, A. Wakif, S. Areekara, A. Mathew, N.A. Shah, Significance of nanoparticles' shape and thermo-hydrodynamic slip constraints on MHD alumina-water nanoliquid flows over a rotating heated disk: the passive control approach, Int. Commun. Heat Mass Tran. 129 (2021), 105711, https://doi.org/10.1016/j.icheatmasstransfer.2021.105711.

[58] M. Alghamdi, A. Wakif, T. Thumma, U. Khan, D. Baleanu, G. Rasool, Significance of variability in magnetic field strength and heat source on the radiative-convective motion of sodium alginate-based nanofluid within a Darcy-Brinkman porous structure bounded vertically by an irregular slender surface, Case Stud. Therm. Eng. 28 (2021), 101428, https://doi.org/10.1016/j.csite.2021.101428.

[59] M. Zaydan, N.H. Hamad, A. Wakif, A. Dawar, R. Sehaqui, Generalized differential quadrature analysis of electro-magneto-hydrodynamic dissipative flows over a heated Riga plate in the presence of a space-dependent heat source: the case for strong suction effect, Heat Transf. 51 (2022) 2063–2078, https://doi.org/10.1002/htj.22388.
[60] L.N. Trefethen, Spectral Methods in MATLAB, SIAM, 2000.
[61] C. Canuto, M.Y. Hussaini, A.M. Quarteroni, A. Thomas Jr., Spectral Methods in Fluid Dynamics, Springer Science & Business Media, 2012.
[62] N. Ishfaq, Z.H. Khan, W.A. Khan, R.J. Culham, Estimation of boundary-layer flow of a nanofluid past a stretching sheet: a revised model, J. Hydrodyn. 28 (2016) 596–602, https://doi.org/10.1016/S1001-6058(16)60663-7.
[63] I.L. Animasaun, R.O. Ibraheem, B. Mahanthesh, H.A. Babatunde, A meta-analysis on the effects of the haphazard motion of tiny/nano-sized particles on the dynamics and other physical properties of some fluids, Chin. J. Phys. 60 (2019) 676–687, https://doi.org/10.1016/j.cjph.2019.06.007.